Ultra-Wideband Double Directional Channel Measurements for THz Communications in Urban Environments

Naveed A. Abbasi*, Jorge Gomez-Ponce*†, Shahid M. Shaikbepari*, Sheryas Rao*, Revanth Kondaveti*,
Shadi Abu-Surra‡, Gary Xu‡, Charlie Zhang‡, Andreas F. Molisch*
* University of Southern California, Los Angeles, CA, USA
†ESPOL Polytechnic University, Escuela Superior Politécnica del Litoral, ESPOL,
Facultad de Ingeniería en Electricidad y Computación, Km 30.5 vía Perimetral, P. O. Box 09-01-5863, Guayaquil, Ecuador
‡ Samsung Research America, Richardson, TX, USA
Email: {nabbasi, gomezpon, shaikbep, srrao, kondavet, molisch}@usc.edu,
{shadi.as, gary.xu, jianzhong.z}@samsung.com

ICC 2021 - IEEE International Conference on Communications | 978-1-7281-7122-7/21/$31.00 ©2021 IEEE | DOI: 10.1109/ICC42927.2021.9500510

***Abstract*—Wireless communications in the THz frequency range can allow data rates of hundreds of Gbit/s, and will thus be an important part of 6G. A first important step for system design is an understanding of the underlying propagation channel. In this paper, we present results from one of the first measurement campaigns for medium-distance (up to 35 m) outdoor channels in urban environments where both the directions and delays of multipath are measured with good resolution. The results show a surprisingly rich multipath environment, leading to significant dispersion in both delay and angular domains. We also find that metallic-covered surfaces lead to a considerable enhancement of multipath, which indicates an important impact of building materials. Overall, the results indicate that relying on pronounced sparsity for THz system design might not always be valid in this type of environment.**

***Index Terms*—Terahertz (THz) communication, urban scenario, Double-directional channel measurements, sparsity**

I. Introduction

As new applications, such as virtual reality, create demand for ultra-high data rates beyond the capabilities of 5G-based mmWave systems [1]–[3], the wireless community naturally turns to higher frequencies, where the spectrum is less congested with existing services and larger bandwidths are available. In particular, the frequency range from 0.1-0.5 THz has been widely explored, e.g., [4]–[10] and is envisioned to be part of 6G wireless systems [11]. This trend has been enhanced by the recent decision of the Federal Communication Commission (FCC) to provide experimental licenses in this band [12].

However, before any such systems can be designed and evaluated, an understanding of the unique propagation conditions in the THz band is required, since they can be significantly different from those at lower frequencies. Higher frequencies are more easily blocked by obstacles, may suffer atmospheric losses, and are reflected more diffusely by many common objects such as trees. Thus, new measurements of the propagation channel characteristics, and measurement-based models, are urgently needed. In particular, since THz systems will use adaptive arrays to overcome the large free-space pathloss isotropic signaling would encounter in this frequency range, the double-directional characteristics of the channel (i.e., impulse responses in particular transmit (Tx) and receive (Rx) directions) are required.

Up to now, most of the interest for THz communications has concentrated on very short range indoor scenarios, such as intra-office links. Consequently, THz propagation channel investigations have concentrated on these scenarios [13]–[17]. However, THz is also of great interest for outdoor wireless access, in particular for hotspot/femtocell scenarios where the distance between Tx and Rx can be up to 100 m. Double-directional channel characteristics are required to analyze performance in particular for non-line-of-sight situations, and/or for investigating the impact of multi-user interference. Yet existing outdoor measurements over this distance are limited to the pathloss/atmospheric attenuation or bit error probabilities for connections where directional horn antennas are pointing into fixed directions, e.g., [18]. The only exception being our recent paper [19], where we saw indications of considerable directional dispersion in the two sample line of sight (LoS) links we analyzed. In the current paper, we provide more extensive results in a somewhat different environment, including both LoS and NLoS (non-LoS) links, and providing for the first time also directional and omni-directional delay dispersion results for these types of links.

The rest of this paper is organized as follows. The measurement setup and site are described in Section II. Section III highlights the major results of our measurement campaign. Finally, the manuscript is concluded in Section IV.

II. Measurement equipment and site

A. Testbed description

Our current work is based on a frequency-domain setup that is shown in Fig. 1. The basic principle of this channel sounder revolves around frequency extension of a vector network analyzer (VNA) signal into the THz domain by means of

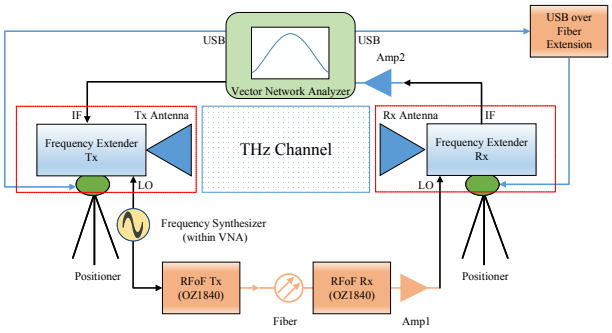

Fig. 1: Channel sounding setup.

frequency multipliers. We introduce a RF-over-fiber (RFoF) link to allow the extension of the Rx beyond the distance limitations of a typical VNA-based THz channel sounding system ($<$ 10 m). This design is similar to the one discussed in our previous work [19] with the difference being that we currently use an integrated RFoF unit to improve the robustness of the design. Due to the measurement principle of mechanically rotating antennas, every measurement lasted for several hours; measurements were done at night to ensure that no movement of people or vehicles was present in the environment. Further details about the setup can be found in [19].

B. Site description

As discussed earlier, the chosen scenario and the environmental characteristics are themselves a very important factor in any channel sounding campaign. For the current measurement, we investigate an outdoor urban scenario. Specifically, our environment is located at the entrance of the Vivian Hall of Engineering (VHE) building in the USC University Park Campus, Los Angeles, CA, USA. It is an open space area with interspersed pillars (see Fig. 2). On both sides of the entrance there are concrete walls and glass doors. The front side faces low height buildings and a street, and the back side faces an open area (quad) with several chairs, tables, trees, and a water fountain (this is the side shown in Fig. 2.b). For all our experiments the Tx and Rx were placed on paved ground.

The reported campaign consisted of 5 measurements in 4 different positions for Tx and Rx where each Tx location has its respective Rx location (Fig.2). For all Links, the height of the Tx and Rx was fixed to 1.65 m to emulate typical device-to-device (D2D) communication links. Link 1 (Tx1-Rx1) constitutes a LoS scenario case where Tx1 is in the northwest corner of the entrance and Rx1 is located at a distance of 29.9 m from it at the opposite side of the entrance. Link 2 (Tx2-Rx2) crosses the entrance diagonally; Tx2 is located at the northeast side of the entrance and Rx2 is located in the southwest corner. For this case, obstacles (i.e., pillars) are present on both sides of the LoS connection and the distance between Tx2 and Rx2 is 34.2 m. Similar to Link 1, Link 3 (Tx3-Rx3) is located on the opposite side of the

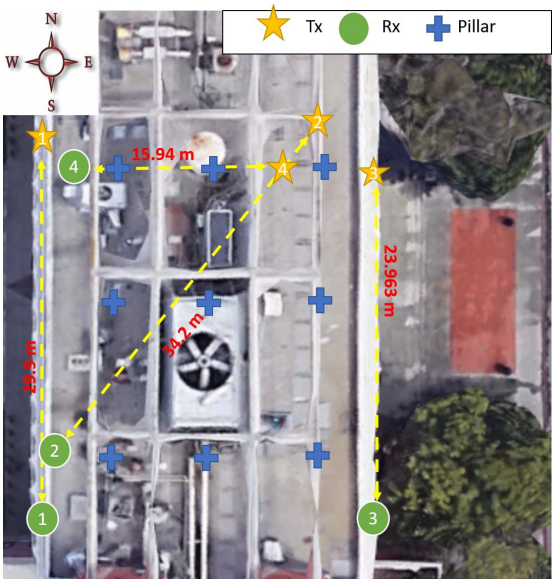

(a) Measurement locations.

entrancev2.eps entrancev2.eps entrancev2.eps

(b) VHE entrance view.

Fig. 2: Measurement scenario description.

entrance to where Link 1 is located, however, the length of this Link is 24.0 m. Note that Link 1 and Link 3 "see" different environments, as Link 3 has buildings on the east side, compared to Link 1 where we have an open area on the west side. Link 4 (Tx4-Rx4) is a NLoS link; for this case Tx and Rx have a geometrical distance of 15.9 m but 2 pillars block the LoS link between them. An additional measurement on Link 4 was performed to analyze the effect of increasing the reflectivity of the obstacles for the NLoS case. For this purpose, we wrapped all the pillars in the scenario with aluminum foil centered at 1.65 m as the antennas and the resulting changes of the channel characteristics generated as a consequence of this modification (see Fig. 3) will be discussed in Sec. III.C.2.

III. Measurement Results

In this section, we present some of our key measurement methodologies and the associated results.

A. Measurement parameters

A summary of key measurement parameters, their acronyms and nominal values is given in Table I. The selection of 1601 frequency points over 1 GHz of bandwidth provides a

(a) Without foil.

(b) With foil.

Fig. 3: Obstacles at VHE entrance.

frequency resolution of 0.62 MHz which translates to 1.6 μs maximum excess delay or 480m excess distance for multipaths to travel. In the current scenario, this is more than sufficient to capture all significant multipath components.

The deployment of the positioners was done such that the angle of 0° for both the Tx and the Rx corresponds to the LoS for Link 1, 2 and 3. Tx and Rx face 90° away from each other in case of Link 4 measurements. The Tx scans a 90° (-45° to 45°) sector of the channel with a resolution of 5° in the azimuth. The Rx on the other hand looks at a full 360° with a 6° angular resolution. Since the antenna beam width is 14°, any resolution below 7° is sufficient for comprehensive channel sounding. It should be noted here that we deliberately kept the elevation of both the Tx and Rx same for the current measurement to simplify the analysis, and since in this particular setup (Tx and Rx at the same height) the significant multipath components can be expected to be in the

TABLE I: Setup parameters.

Parameter	Symbol	Value
Measurement points	N	1601
Start frequency	f_{start}	145 GHz
Stop frequency	f_{stop}	146 GHz
Bandwidth	BW	1 GHz
IF Bandwidth	IF_{BW}	1 KHz
THz IF	f_{THzIF}	279 MHz
Antenna 3dB Beamwidth	θ_{3dB}	13°
Tx rotation range	Tx_{AZ}	[0°,90°]
Tx rotation resolution	ΔTx_{AZ}	5°
Rx rotation range	Rx_{AZ}	[0°,360°]
Tx rotation resolution	Tx_{AZ}	6°

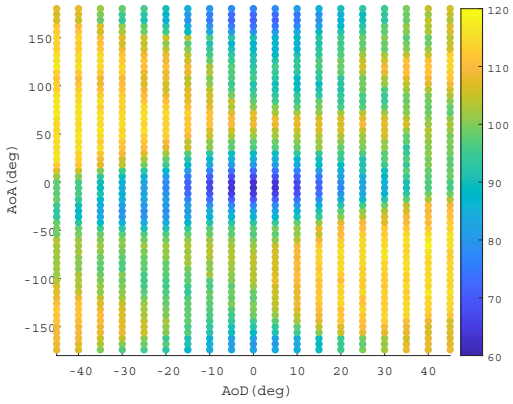

(a) Full capture.

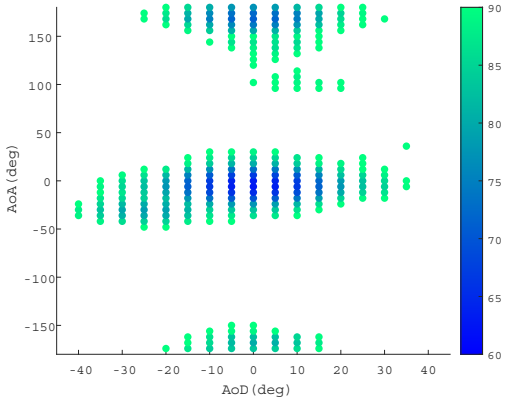

(b) Clusters within 30 dB of LoS.

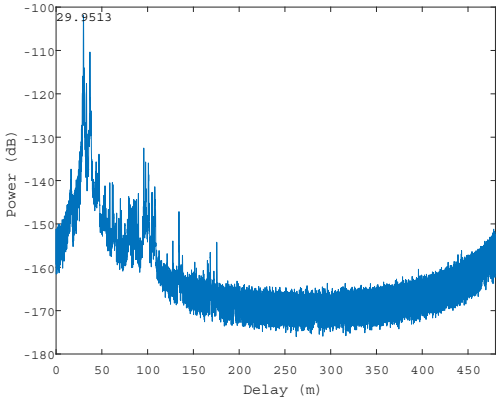

(c) Omni-directional PDP of Link 1 for clusters within 30 dB of LoS.

Fig. 4: Average pathloss per direction pair, clusters and PDP for Link 1.

horizontal plane.

B. LoS measurements

1) Link 1: We first investigate the double-directional power angular spectrum, i.e., the power received for each combination of Tx and Rx direction. Fig. 4 (a) shows the result with the full measured dynamic range (60 dB). Not surprisingly, most

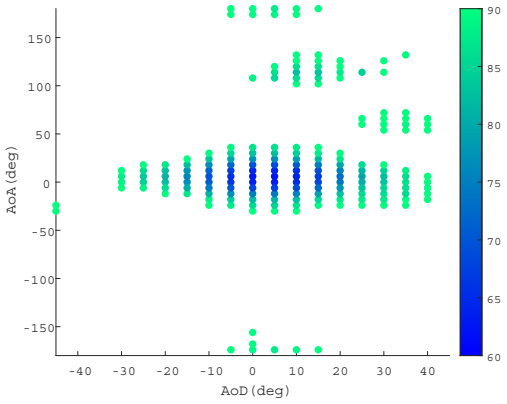

(a) Double-directional power spectrum within 30 dB of the LoS.

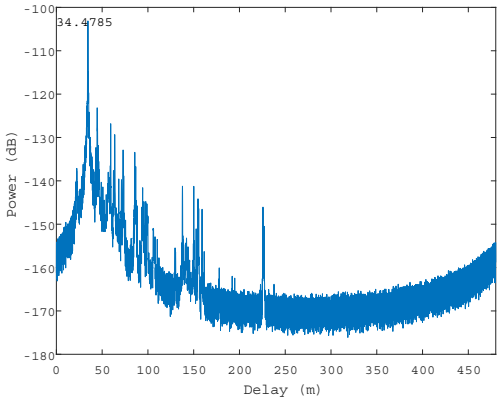

(b) Omni-directional PDP for clusters within 30 dB of LoS.

Fig. 5: Clusters and PDP for Link 2.

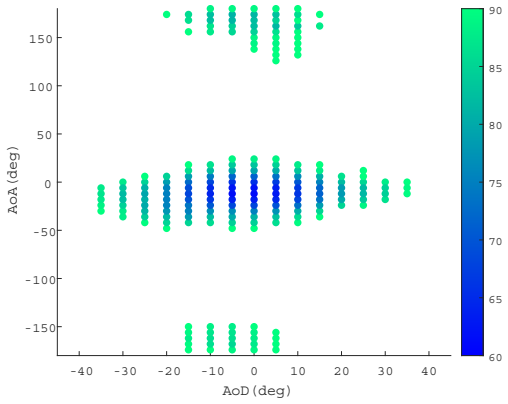

(a) Clusters within 30 dB of LoS.

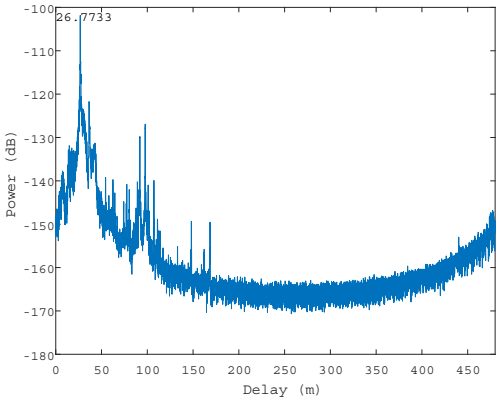

(b) Omni-directional PDP for clusters within 30 dB of LoS.

Fig. 6: Clusters and PDP for Link 3.

of the signal with high power is located around the LoS. Other regions of higher power are concentrated around the back of the Rx (-150° to 150°). To see these effects more clearly, we employ a 30 dB threshold below the LoS, corresponding to the dynamic range of a typical communication receiver. The result is shown in Fig. 4 (b). Here again, we see that apart from strong LoS signal, we have strong reflections from the wall behind the Rx as well. Apart from these, we also see a smaller third cluster centered at almost 100° AoA and 10° AoD. This smaller cluster represents reflections off the pillar nearest to Rx as shown in the site map in Fig. 2. An omni-directional power delay profile (PDP), i.e., integrating the power delay profiles of the different horn orientations in Fig. 4 (b) is shown in Fig. 4 (c). Following [20], it is calculated by collecting the maximum power component in each delay bin from the (reduced) snapshot and adding them together. We see that the biggest peak corresponds to the LoS link and the distance (converted from the measured delay by multiplying with the speed of light) for this peak corresponds to our measurements from the scenario. A number of other multipaths are also observed in channel that correspond to various reflective surfaces in the scenario with excess lengths of up to 150 m.

Before we move on to the next links, we note that since thresholding of the snapshot more easily visualizes information about key regions of low loss, we will only look at these reduced snapshots for the rest of the links instead of the complete snapshots.

2) Link 2: The major clusters for Link 2 are shown in Fig. 5 (a). Although we do have a LoS cluster similar to Link 1, in this case we have only weak reflections from the back. The main reason for this is that instead of a wall on the back of Rx, in this case, we have some vegetation that does not have create strong specular reflections. Apart from this, we also see two other smaller clusters that correspond to reflections that go from the pillars to the buildings and finally end up at the Rx. The omni-directional PDP in Fig. 5 (b) again shows the strongest peak from the LoS signal at a distance corresponding to the geometric distance, as shown in the scenario map in Fig. 2. We see a higher number of multipaths, some of which have runlength greater than 200 m. This is because in this case we have a larger number of reflectors in the form of buildings and pillars available within the Tx's 90° sector.

3) Link 3: Fig. 6 shows the clusters and omni-directional PDP for Link 3. The results are similar to those of Link 1 with strong LoS and a back-reflection clusters. The major difference

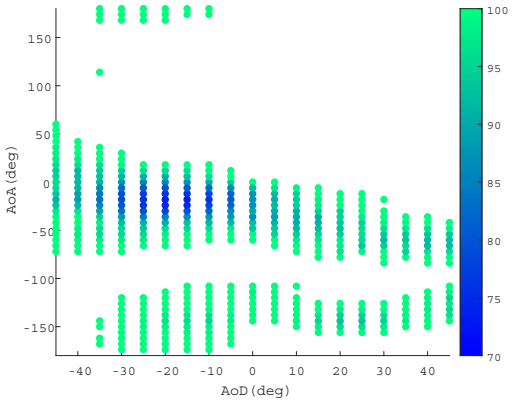

(a) Clusters 30 dB below maximum power.

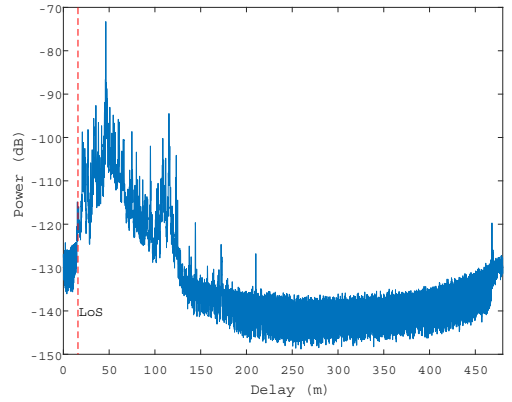

(b) Omni-directional PDP for clusters 30 dB below maximum power.

Fig. 7: Clusters and PDP for Link 4 without reflective foil.

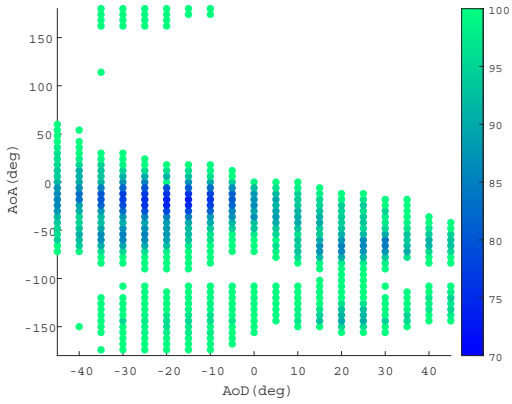

(a) Clusters 30 dB below maximum power.

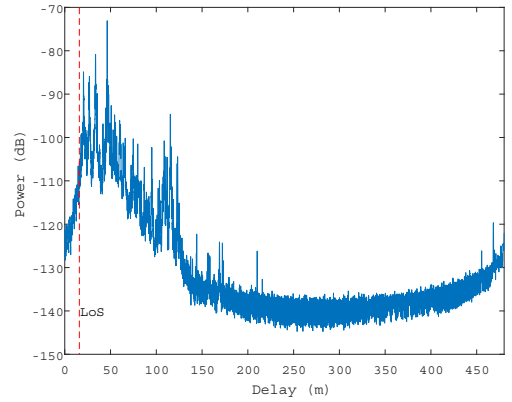

(b) Omni-directional PDP for clusters 30 dB below maximum power.

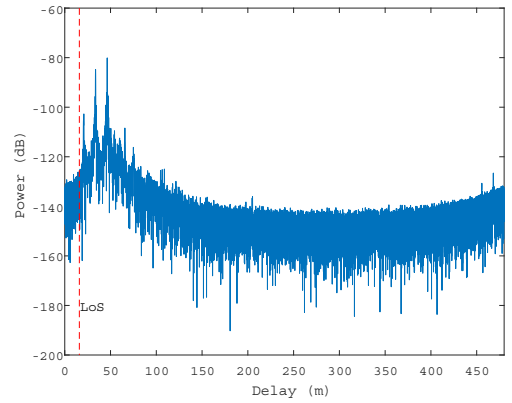

(c) Sample directional PDP Tx -30° and Rx -24°.

Fig. 8: Clusters and PDPs for Link 4 with reflective foil.

is the absence of a pillar reflection similar to the one scene in Link 1. The reason for that is that propagation is along a road that has a thick cover of vegetation that blocks the connection from Tx to pillars. The PDP is similar to that of Link 1.

C. NLoS measurements

1) Without reflective foil: The results for NLoS measurements of Link 4 without any reflective foil in the environment are shown in Fig. 7. We see that even in this case several major clusters are present in the environment. From the 1140 direction pairs of Tx and Rx, we receive significant power in 411 pairs. These are all reaching the Rx through a number of paths in the channel. The PDP in Fig. 7 (b) does shows a very high multipath richness. The strongest path arrives after a detour of 46.35 m in the channel whereas there is no component at the LoS delay (≈16 m) since a pillars blocks the LoS, and the Rx is not in the 90° sector that the Tx illuminates.

2) With reflective foil: We now investigate whether multipath richness of the channel is further increased by the use of more reflective surfaces on various structures in the environment. As described in Sec. II, to achieve this, we use reflective foil on the pillars in the scenario. The increase in the number of significant (within 30 dB of the peak) direction pairs can be visually established by comparing Fig. 7 (a) and Fig. 8 (a). In all, 484 direction pairs have significant power, which is 73 more than the previous case. This shows that the use of reflective foil can significantly increase the multipath richness of the channel. The same can also be seen in the omni-directional PDP where we not only have more multipaths but also their power is higher than the previous case. We show a sample directional PDP in Fig. 8 (c) for -30° and Rx -24° to

see the multipath characteristics of individual directions. We see that, similar to the omni-PDP, the directional PDP also exhibits multipath richness where a number of components are clearly visible.

Turning now to the statistics of the channel, we investigate the RMS angular spreads. Using the definition of angular spread in [21], we calculate the angular spreads shown in Table II. The Rx spreads are relatively larger because the signal has had a chance to spread over the long channel length. The angular spreads are similar to our previous paper ([19]) where a 100 m distance Tx-Rx was measured. Note that according to the definition of [21], the maximum angular spread can be unity.

TABLE II: RMS angular spread for various links, computed according to definition of [21].

Parameter	Link 1	Link 2	Link 3	Link 4 no foil	Link 4 with foil
$\mathbf{S}_{AoA}$	0.9591	0.8439	0.8029	0.8070	0.7842
$\mathbf{S}_{AoD}$	0.2815	0.2833	0.3009	0.3728	0.3906

IV. Conclusion

In this paper, we reported results of a double-directional (i.e., directional resolution at both link ends), ultra-wideband (1 GHz bandwidth) measurement campaign at 145 GHz carrier frequency. Measurements are done for D2D setups in an outdoor urban environment, with distances of 15-35 m between Tx and Rx. We found, surprisingly, a considerable multipath richness within a 30 dB dynamic range of the peak received amplitude. This is important not only for assessing the sensitivity of the communications links to dispersion, but also for the treatment of multi-user interference, in particular since the near-far effect might enhance the effect of multipath components of interfering users.

We also found that the specifics of the environment play a major role - concrete walls lead to much stronger reflections than vegetation, pillars and similar structures can be significant reflectors, and the building material impacts reflection coefficients and thus overall multipath richness, with metallic coating (which is used, e.g., in energy-saving windows) reflecting much more strongly than, e.g., concrete surfaces.

These results and insights can help in the design of THz communications systems and in particular indicate that channel sparsity (in the sense of only a small number of multipath components), which is often used in theoretical investigations at high frequencies, might not hold in at least some environments of interest.

Acknowledgments

The work of USC was partly supported by the Semiconductor Research Corporation (SRC) under the ComSenTer program and by Samsung Research America. The work of J. Gomez-Ponce is partially supported by the Foreign Fulbright Ecuador SENESCYT Program.

References

[1] K.-C. Huang and Z. Wang, "Terahertz Terabit Wireless Communication," *Microwave Magazine, IEEE*, vol. 12, no. 4, pp. 108–116, June 2011.

[2] V. Chandrasekhar, J. G. Andrews, and A. Gatherer, "Femtocell networks: a survey," *IEEE Communications Magazine*, vol. 46, no. 9, pp. 59–67, September 2008.

[3] M. Shafi, A. F. Molisch, P. J. Smith, T. Haustein, P. Zhu, P. D. Silva, F. Tufvesson, A. Benjebbour, and G. Wunder, "5G: A Tutorial Overview of Standards, Trials, Challenges, Deployment and Practice," *IEEE Journal on Selected Areas in Communications*, 2017.

[4] A. Hirata and M. Yaita, "Ultrafast Terahertz Wireless Communications Technologies," *IEEE Transactions on Terahertz Science and Technology*, vol. 5, no. 6, pp. 1128–1132, Nov 2015.

[5] I. F. Akyildiz, J. M. Jornet, and C. Han, "TeraNets: ultra-broadband communication networks in the terahertz band," *IEEE Wireless Communications*, vol. 21, no. 4, pp. 130–135, August 2014.

[6] H. J. Song and T. Nagatsuma, "Present and Future of Terahertz Communications," *IEEE Transactions on Terahertz Science and Technology*, vol. 1, no. 1, pp. 256–263, Sept 2011.

[7] T. Kürner and S. Priebe, "Towards THz Communications - Status in Research, Standardization and Regulation," *Journal of Infrared, Millimeter, and Terahertz Waves*, vol. 35, no. 1, pp. 53–62, 2014.

[8] I. F. Akyildiz, J. M. Jornet, and C. Han, "Terahertz band: Next frontier for wireless communications ," *Physical Communication*, vol. 12, pp. 16 – 32, 2014.

[9] N. A. Abbasi, A. Hariharan, A. M. Nair, and A. F. Molisch, "Channel measurements and path loss modeling for indoor thz communication," in *2020 14th European Conference on Antennas and Propagation (EuCAP)*. IEEE, 2020, pp. 1–5.

[10] N. A. Abbasi, A. F. Molisch, and J. C. Zhang, "Measurement of directionally resolved radar cross section of human body for 140 and 220 ghz bands," in *2020 IEEE Wireless Communications and Networking Conference Workshops (WCNCW)*. IEEE, 2020, pp. 1–4.

[11] H. Tataria, M. Shafi, A. F. Molisch, M. Dohler, H. Sjöland, and F. Tufvesson, "6g wireless systems: Vision, requirements, challenges, insights, and opportunities," 2020.

[12] FCC, "Fcc takes steps to open spectrum horizons for new services and technologies," http://https://docs.fcc.gov/public/attachments/DOC-356588A1.pdf, 2019.

[13] M. Y.-W. Chia, B. Luo, and C. K. Ang, "Extremely wideband multipath propagation channel from 285 to 325 ghz for a typical desk-top environment," in *Infrared Millimeter and Terahertz Waves (IRMMW-THz), 2010 35th International Conference on*. IEEE, 2010, pp. 1–1.

[14] S. Priebe, C. Jastrow, M. Jacob, T. Kleine-Ostmann, T. Schrader, and T. Kürner, "Channel and propagation measurements at 300 GHz," *Antennas and Propagation, IEEE Transactions on*, vol. 59, no. 5, pp. 1688–1698, 2011.

[15] S. Kim and A. G. Zajić, "Statistical characterization of 300-ghz propagation on a desktop," *IEEE Transactions on Vehicular Technology*, vol. 64, no. 8, pp. 3330–3338, 2015.

[16] S. Kim and A. Zajić, "Characterization of 300-ghz wireless channel on a computer motherboard," *IEEE Transactions on Antennas and Propagation*, vol. 64, no. 12, pp. 5411–5423, 2016.

[17] N. Khalid, N. A. Abbasi, and O. B. Akan, "Statistical characterization and analysis of low-thz communication channel for 5g internet of things," *Nano Communication Networks*, vol. 22, p. 100258, 2019.

[18] J. Ma, R. Shrestha, L. Moeller, and D. M. Mittleman, "Invited article: Channel performance for indoor and outdoor terahertz wireless links," *APL Photonics*, vol. 3, no. 5, p. 051601, 2018.

[19] N. A. Abbasi, A. Hariharan, A. M. Nair, A. S. Almaiman, F. B. Rottenberg, A. E. Willner, and A. F. Molisch, "Double directional channel measurements for thz communications in an urban environment," in *ICC 2020-2020 IEEE International Conference on Communications (ICC)*. IEEE, 2020, pp. 1–6.

[20] C. U. Bas, R. Wang, S. Sangodoyin, S. Hur, K. Whang, J. Park, J. Zhang, and A. F. Molisch, "28 ghz foliage propagation channel measurements," in *2018 IEEE Global Communications Conference (GLOBECOM)*, 2018, pp. 1–6.

[21] B. H. Fleury, "First-and second-order characterization of direction dispersion and space selectivity in the radio channel," *IEEE Transactions on Information Theory*, vol. 46, no. 6, pp. 2027–2044, 2000.